

Cite this: *Biomater. Sci.*, 2022, **10**, 6768

N-Cadherin adhesive ligation regulates mechanosensitive neural stem cell lineage commitment in 3D matrices†

Jieung Baek, ^{a,b} Sanjay Kumar, ^{a,b,c} David V. Schaffer^{a,b,d} and Sung Gap Im ^{*e}

During differentiation, neural stem cells (NSCs) encounter diverse cues from their niche, including not only biophysical cues from the extracellular matrix (ECM) but also cell–cell communication. However, it is still poorly understood how these cues cumulatively regulate mechanosensitive NSC fate commitment, especially in 3D matrices that better mimic *in vivo* systems. Here, we develop a click chemistry-based 3D hydrogel material system to fully decouple cell–cell and cell–ECM interactions by functionalizing small peptides: the HAVDI motif from N-cadherin and RGD motif from fibronectin. The hydrogel is engineered to range in stiffness from 75 Pa to 600 Pa. Interestingly, HAVDI-mediated interaction shows increased neurogenesis, except for the softest gel (75 Pa). Moreover, the HAVDI ligation attenuates the mechanosensing state of NSCs, exhibiting restricted cytoskeletal formation and RhoA signaling. Given that mechanosensitive neurogenesis has been reported to be regulated by cytoskeletal formation, our finding suggests that the enhanced neurogenesis in the HAVDI-modified gel may be highly associated with the HAVDI interaction-mediated attenuation of mechanosensing. Furthermore, NSCs in the HAVDI gel shows higher β -catenin activity, which has been known to promote neurogenesis. Our findings provide critical insights into how mechanosensitive NSC fate commitment is regulated as a consequence of diverse interactions in 3D microenvironments.

Received 24th August 2022,
Accepted 15th October 2022

DOI: 10.1039/d2bm01349e

rsc.li/biomaterials-science

1. Introduction

Neural stem cells (NSCs) have critical potential for both regenerative medicine and a model system to understand development and disease,^{1–4} and their lineage commitment is regulated by intricate instructive signals from the cellular microenvironment or niche, including soluble factors,^{5,6} extracellular matrix (ECM),^{7–9} factors immobilized to the ECM,¹⁰ and cues from neighboring cells.^{11–14} In particular, recent progress demonstrates that not only the biochemical signals but also biophysical properties of the niche – especially the mechanical properties of the microenvironment – are key determinants of cell

behavior.^{9,15,16} It has been increasingly recognized that the mechanical properties of ECM modulate cytoskeletal tension and activate mechanotransductive signaling complexes^{15–17} to regulate NSC fate decisions.^{18–22} For example, in our previous work, we found that NSC lineage commitment is regulated by the mechanical stiffness of three-dimensional (3D) matrices through a 3D matrix-specific mechanism.⁹ This was mediated by mechanosensitive cytoskeletal formation and early growth response 1 (*Egr1*) expression. In addition to such mechanical cues from ECM, cell–cell interactions can regulate NSC differentiation. For example, N-cadherin, a cell adhesion molecule mediating calcium-dependent homophilic cell–cell adhesions, has been known to play important roles during neurogenesis.¹⁴ It has been reported that N-cadherin-mediated cell–cell interaction of rat embryonic NSCs enhances proliferation and neuronal differentiation by upregulating the expression of brain derived neurotrophic factor (BDNF) and neurotrophin (NT-3).¹²

However, biophysical cues and cell–cell interactions have the potential to work not only independently but also in combination with each other. Thus, several strategies have been used to investigate the effect of cell–cell interactions on cellular response to the biophysical cues: modulating cell density^{23,24} or cell clustering¹² and integrating optimal presentation of recombinant adhesive proteins involved in cell–cell

^aDept. of Chemical and Biomolecular Engineering, University of California, Berkeley, Berkeley, CA 94720, USA

^bDept. of Bioengineering, University of California, Berkeley, Berkeley, CA 94720, USA

^cDept. of Bioengineering and Therapeutic Sciences, University of California, San Francisco, San Francisco, CA 94158, USA

^dDept. of Molecular and Cell Biology, University of California, Berkeley, Berkeley, CA 94720, USA

^eDept. of Chemical and Biomolecular Engineering, Korea Advanced Institute of Science and Technology (KAIST), Daejeon 34141, Republic of Korea.

E-mail: sgim@kaist.ac.kr

† Electronic supplementary information (ESI) available. See DOI: <https://doi.org/10.1039/d2bm01349e>

interactions.^{13,14} However, the former systems based on cell clustering cannot provide cell–cell interaction cues homogeneously to all cells. Furthermore, for the presentation strategies, it is challenging to fully decouple the effects of cell–cell and cell–other niche interactions: within a constant substrate area, increased presentation of cell–cell interaction cues consequently results in a decreased presentation of the other signaling cues. Above all, most of these systems have been applied to 2D substrates, though cells in 3D microenvironments exhibit different mechanosensing processes, and such systems may better mimic *in vivo* biology.^{9,25–29} That said, 3D hydrogel encapsulation has limitations: (1) it typically isolates cells from one another to control the cues homogeneously to all the cells and (2) it is comparatively more difficult to functionalize 3D hydrogels with whole recombinant adhesive macromolecules to modulate for cell–cell interactions without significant alternation in the hydrogel characteristics.

Here, we jointly presented small peptide sequences to emulate both N-cadherin-mediated cell–cell interaction and integrin-mediated cell–ECM interaction in 3D matrices: the HAVDI adhesive motif from EC1 domain of N-cadherin^{30–33} and an RGD adhesive motif from fibronectin. Both peptides containing azide group at the end of the sequences were functionalized to the hydrogels based on hyaluronic acid (HA), a major component of brain ECM,^{7,34} through a strain-promoted azide alkyne cycloaddition (SPAAC) click reaction.^{9,35} In RGD-functionalized gels without HAVDI, neuronal differentiation was lower in stiffer 3D matrices, consistent with NSC mechanosensitivity observed in our previous work.⁹ On the other hand, interestingly, HAVDI-mediated N-cadherin adhesive ligation rescued the lower neurogenesis in stiffer 3D gels. In addition, the HAVDI interaction restricted cytoskeletal formation and RhoA signaling, which have previously been shown to limit neuronal differentiation in stiffer gels.^{9,16} Moreover, the N-cadherin ligation resulted in increased activity of β -catenin, which has been known as a master-regulator of cell fate during neurogenesis.^{36,37} Taken together, our findings offer the novel observation that mechanosensitive NSC behaviors derived from cell–ECM interaction can be altered through cell–cell interaction-mediated shielding of mechanosensing.

2. Results and discussion

2.1. Neurogenesis is mechanosensitive and facilitated when the cells are aggregated in 3D matrices

To observe the lineage commitment of human neural stem cell (hNSC) derived from fetal telencephalon (HFT13)³⁸ in a 3D hydrogel, we covalently conjugated dibenzocyclooctyne (DBCO) to HA through *N*-hydroxysuccinide (NHS)-*N*-(3-dimethylaminopropyl)-*N'*-ethylcarbodiimide (EDC) chemistry (ESI Fig. S1A and B†). Then, we used the DBCO-ligated HA (HA-DBCO) as a backbone and polyoxyethylene bis(azide) (PEG-bis(azide)) as a crosslinker to synthesize a series of HA hydrogels based on strain-promoted alkyne–azide cycloaddition (SPAAC) click chemistry.^{9,35,39} In addition, pendant, azide-conju-

gated RGD peptides [K(N₃)GSGRGDSPG] at the concentration of 1 mM were added to induce integrin–ECM interaction. We have previously found 1 mM to be a sufficient concentration to engage NSCs in the same gels.⁹ Incubation of the mixture containing all the reagents plus hNSCs for 10 min at 37 °C enabled 3D encapsulation of the cells (Fig. 1A). We next optimized the HA concentration for maintaining cell viability. Cell viability in the gels with 3 wt% of HA decreased to 59.36% after 7 days of encapsulation. On the other hand, gels with 2 wt% of HA exhibited 94% and 78% cell viability at days 1 and 7, respectively, indicating that there is no striking effect of 3D encapsulation with 2 wt% of HA on cell viability for up to 7 days (Fig. 1B and C). Maintaining the HA concentrations at 2 wt%, we engineered the hydrogels to range in stiffness from 90 Pa to 1000 Pa by controlling molar ratio of azide groups in PEG-bis(azide) to HA monomers from 0.02 to 0.05 (Fig. 1D). The swelling ratio of the 90-Pa gels and 1000-Pa gels were not significantly different with each other (ESI Fig. S1C†) and their mesh sizes in the polymer network were in the order of $\sim 10^2$ nm (ESI Fig. S1D†). This is consistent with a previous finding that HA-based hydrogels in this stiffness range (90 Pa–1000 Pa) are nanoporous with the mesh sizes on the order of $\sim 10^2$ nm.^{40,41} These pore scales are smaller than cells and neurites,^{4,42} such that variation of mesh size would not be expected to strongly influence cell volumetric expansion or outgrowth.

Next, we investigated whether hNSC lineage commitment depends on the stiffness of 3D matrices within a range from 90 Pa to 600 Pa, in which the cells did not show a significant difference in total differentiation (Fig. 1E and F). The cells were differentiated for 7 days within the 3D gels with three different stiffnesses (90 Pa, 250 Pa, and 600 Pa), then fixed and stained for neuronal (neuron-specific class III β -tubulin, β -tubulin III) and astrocytic (glial fibrillary acidic protein, GFAP) lineage markers to quantify the lineage commitment. Differentiation was biased towards neurons in softer gels (90 Pa) and astrocytes in stiffer gels (600 Pa), showing a stiffness-dependence of lineage distribution. Our gelation encapsulates gels in a 3D microenvironment rapidly enough to preventing them from sinking to the bottom during gelation (ESI Fig. S2†), such that our results confirm that fate commitment of hNSCs is mechanosensitive in 3D matrices. This correlates well with our previous finding with rat hippocampal adult NSCs.⁹ The same trend has also been observed with other neural stem cell lines and other 3D hydrogel materials,^{18,22} demonstrating that the mechanosensitive neurogenesis is not a feature specific to human fetal neural stem cells or HA hydrogels. As a potential mediator for this stiffness-dependent neurogenesis, RhoA signaling is known to be central to mechanotransduction and primarily associated with cytoskeleton regulation and actomyosin contractility.^{43,44} We have previously found that RhoA signaling is activated on stiff 2D substrates and inhibits NSC neuronal differentiation.¹⁶ Consistent with these findings, we found that neurogenesis in all gels was reversed by treatment with a selective Rho-associated kinase (ROCK) inhibitor (Y27632), resulting in no significant difference in neurogenesis between the gels with all the stiffnesses

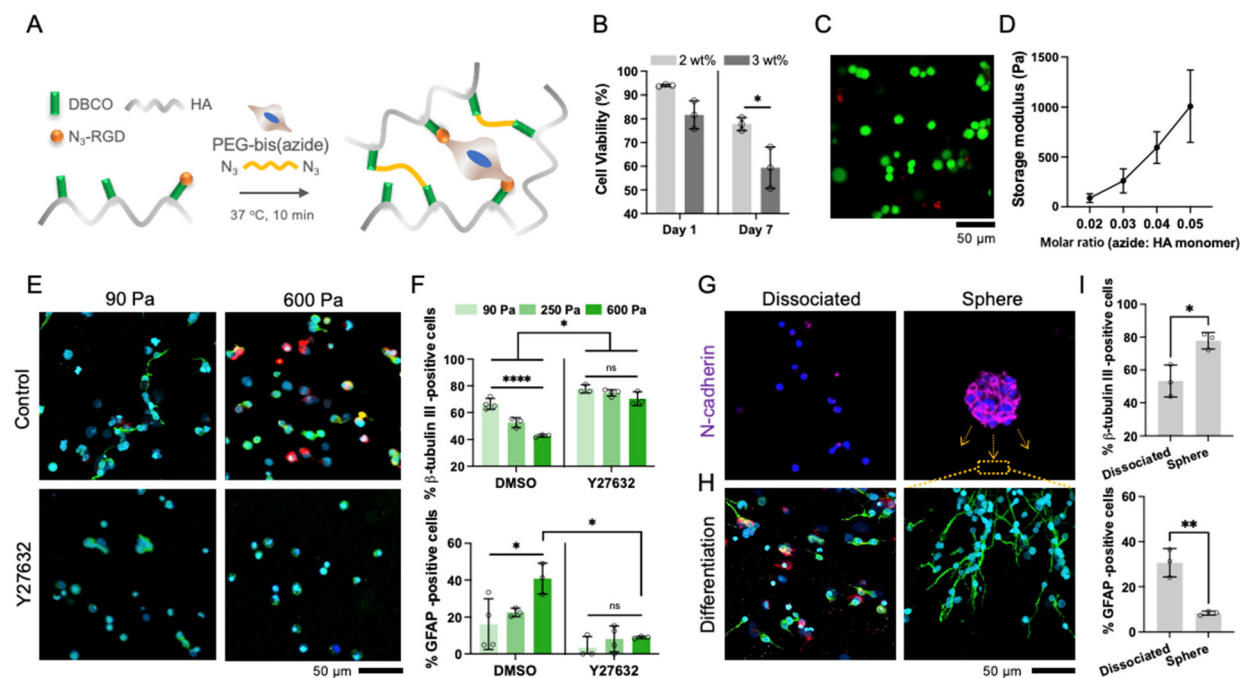


Fig. 1 Neurogenesis is mechanosensitive and facilitated when the cells are aggregated in 3D matrices. (A), Schematic illustration of 3D encapsulation of hNSCs with HA-DBCO hydrogel. $n > 137$ cells per condition. (B), Quantification of Live/Dead cell viability assay with hNSCs within HA-DBCO 3D gels (2 wt% or 3 wt% of HA in total gel solution, 600 Pa) at day 1 and day 7. (C), Confocal stacked image of the Live/Dead assay of hNSCs in 2 wt% HA gels at day 1, showing live cells stained with Calcein-AM (green) and dead cells with EthD-1 (red). Scale bar, 50 μm . (D), Elastic moduli of HA-DBCO hydrogels measured with different molar ratio of azide to HA monomer. $n > 3$. (E), Immunofluorescence staining and (F), lineage marker-positive percentage of hNSCs differentiated into neuronal (β -tubulin III, green) and astrocyte (GFAP, red) lineages in 3D gels with different elastic moduli for 7 days under DMSO- or Y27632-treated condition. $n = 3$ biological replicates. Scale bar, 50 μm . $n > 66$ cells per condition. (G), Immunofluorescence staining of N-cadherin in isolated (dissociated) or aggregated (sphere) cells in 3D gels (250 Pa). Scale bar, 50 μm . (H), Immunofluorescence staining of each lineage marker (β -tubulin III, green; GFAP, red) of the dissociated or sphere cells differentiated in 3D gels for 7 days and (I), quantification of each marker-positive cells. $n = 3$ biological replicates. $n > 183$ cells per condition. One-way ANOVA followed by Tukey test (B and F) or Student's t -test (I). **** $P < 0.001$, *** $P < 0.005$, ** $P < 0.01$, * $P < 0.05$. Graphs show means \pm SD.

(Fig. 1E and F) and suggesting that Rho/ROCK signaling may play a role in the mechanosensitive lineage commitment within 3D gels.

We next examined whether cell aggregation, which induces more cell–cell interactions, alters the lineage distribution in the same 3D matrices. The cells were encapsulated as single cells after dissociation (dissociated) or as aggregates (spheres) within 250-Pa hydrogels. After 24 h of encapsulation, cell spheres exhibited higher expression of N-cadherin, especially at cell–cell junctions, than dissociated cells (Fig. 1G). In addition, interestingly, neuronal differentiation was higher in spheres than in dissociated cells after 7 days of differentiation, whereas astrogenesis showed the opposite trend (Fig. 1H and I). These results demonstrate that cell–cell interactions may promote neurogenesis in 3D matrices.

2.2. N-Cadherin adhesive ligation enhances neurogenesis in 3D stiffer matrices

To assess the potential role of N-cadherin-mediated cell–cell interaction in mechanosensitive NSC lineage commitment, we additionally incorporated azide-containing small peptides to the RGD-ligated HA-DBCO gels: HAVDI [Ac-K(N₃)-

HAVDIGGG-NH₂] motif for N-cadherin adhesive ligation or non-functional scrambled HAVDI [Ac-K(N₃)-AGVGDHIGC-NH₂] for preserving the same level of HA-DBCO functionalization (Fig. 2A). We functionalized these peptides at a concentration of 1 mM, which has been known as within the range of previous measures of cadherin density in developing *Drosophila* embryos and monolayer epithelial cells.⁴⁵ We confirmed the incorporation of both peptides (HAVDI and scrambled HAVDI) to HA-DBCO gels by fluorescence tagging and visualizing them after washing (ESI Fig. S3[†]). Presentation of scrambled HAVDI for control gels (SCR gel), which presumably does not induce cadherin-based interactions, enabled a similar elastic modulus to that of HAVDI-modified gels (HAV gel) at the same molar ratio of azide (crosslinker) to HA monomers from 0.02 to 0.04 (Fig. 2B).

We next verified whether this HAVDI presentation faithfully recruits N-cadherin and enables hNSC engagement. Immunofluorescence staining for N-cadherin revealed that hNSCs in HAV gels exhibited higher expression of N-cadherin at the cell membrane than in SCR gel (ESI Fig. S4[†]). Moreover, hNSCs were seeded onto gels functionalized with each peptide (1 mM) solely to determine whether hNSCs adhered to each

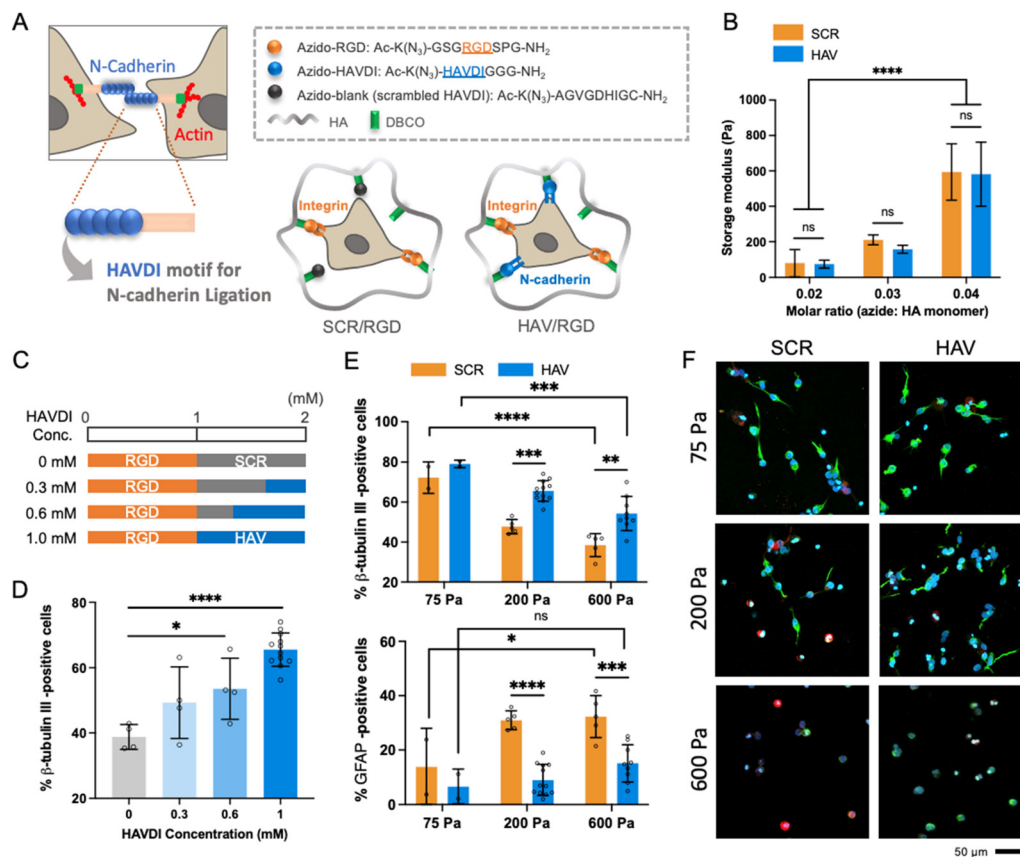


Fig. 2 N-Cadherin adhesive ligation enhances neurogenesis in 3D matrices. (A), Schematic illustrating of azido-peptides (RGD for integrin binding, HAVDI for N-cadherin adhesive ligation, scrambled HAVDI) functionalization to HA-DBCO gels to induce N-cadherin adhesive ligation. (B), Elastic moduli of SCR/RGD (SCR) and HAV/RGD (HAV) gels with different molar ratios of azide to HA monomer. $n > 10$. (C), Composition of functionalized azido-peptides in gels with different HAVDI concentration (0 mM, 0.3 mM, 0.6 mM, 1 mM). RGD concentration was kept as 1 mM for all the gels. (D), Quantification of β -tubulin III-positive cells differentiated in 3D gels with the four different HAVDI concentrations. $n = 3$ biological replicates. $n > 99$ cells per condition. (E), Quantification of β -tubulin III (top)- and GFAP (bottom)-positive cells differentiated for 7 days in SCR (1 mM) or HAV (1 mM) gels with three different stiffnesses (75 Pa, 200 Pa, and 600 Pa). $n = 3$ biological replicates. $n > 47$ cells per condition. (F), Immunofluorescence staining of hNSCs differentiated in the SCR and HAV gels with the three different stiffnesses: neuronal lineage (β -tubulin III), green; astrocyte lineage (GFAP), red. Scale bar, 50 μ m. One-way ANOVA followed by Tukey test. **** $P < 0.001$, *** $P < 0.005$, ** $P < 0.01$, * $P < 0.05$. Graphs show means \pm SD.

single peptide: scrambled HAVDI, HAVDI, RGD, and non-functionalized (no peptide) (ESI Fig. S5A and B[†]). After 24 h, hNSCs adhesion to each gel was determined by measuring the number of the cells attached on the gels after washing, and the % cell attachment was obtained by quantifying the number % of adhered cells relative to the number of initially seeded cells. Only a small level of cell attachment (about 10%) was observed on both no peptide gels and scrambled HAVDI gels. Since NSCs have been known to interact with HA by several non-integrin surface receptors, such as CD44, RHAMM, and TLR2/4,⁷ the small amount of attachment despite a lack of peptide presentation could be due to cell-HA interactions mediated by such receptors. Consistently, blocking of CD44 prevented cell adhesion on 2D HA gels without RGD (ESI Fig. S5C[†]), and the CD44-blocked cells showed less protrusion in 3D gels without RGD than unblocked (control) cells (ESI Fig. S5D[†]). These results strongly support that CD44 functions in cellular engagement to bare HA gels. Furthermore, cell attachment to the scrambled HAVDI-modified gels was not sig-

nificantly different from that of no peptide gels, meaning that the scrambled HAVDI itself does not support cell attachment (ESI Fig. S5A and B[†]). In contrast, HAVDI-modified gels showed higher cell attachment when compared with either no peptide gels or scrambled HAVDI-modified gels, though the level was lower than that to RGD-modified gels. The first two extracellular domains of N-cadherin, where the HAVDI sequence resides, may mediate lower adhesive interactions compared to the full ectodomain.⁴⁶ In sum, these results substantiate that hNSCs specifically adhere to HAVDI peptide as well as RGD.

We next examined whether this HAVDI-mediated ligation influences hNSC fate commitment in 3D matrices. To assess hNSC differentiation on the HAVDI gels, starting with a standard 1 : 1 ratio of RGD to HAVDI peptide, increasing levels of the latter were titrated (from 0 mM to 1 mM) (Fig. 2C). Intriguingly, the proportion of β -tubulin III-positive cells, assessed *via* immunofluorescent staining, revealed a strong HAVDI peptide dose-dependence, with increasing neurogen-

esis at higher HAVDI incorporation at the constant stiffness of 200 Pa (Fig. 2D). Furthermore, we investigated whether this effect is dependent on the stiffness of the gels by comparing SCR gels and HAV gels at three different stiffnesses: 75 Pa, 200 Pa, and 600 Pa. The concentration of RGD peptide was kept as 1 mM for all the gels and 1 mM of HAVDI or scrambled HAVDI peptide was incorporated to the RGD-containing gels to make HAV or SCR gels, respectively. Notably, stiffer gels (200 Pa and 600 Pa) reversed the effects of HAVDI and restored lower neurogenesis, whereas 75 Pa gels did not show significant difference in neuronal differentiation between SCR and HAV gels (Fig. 2E and F). Astrocytic differentiation exhibited a similar trend on HAVDI gels: a decrease in astrogenesis with HAVDI modification only in 200- and 600-Pa gels. Consequently, the astrogenesis within HAVDI-incorporated gels did not show a statistically significant stiffness dependence. These indicate that HAVDI-mediated adhesion promotes fate commitment towards neuronal lineage, and this happens only in stiffer gels, not in soft gels (75 Pa).

2.3. HAVDI-mediated adhesion restricts cytoskeletal formation and RhoA activity

To investigate how HAVDI adhesion regulates neurogenesis in a mechanosensitive manner, we first examined cytoskeletal formation, which has previously been found to be more pronounced in stiffer 3D gels.⁹ We quantified F-actin intensity

from the images of phalloidin-stained hNSCs in SCR or HAV gels at the stiffness that showed the most statistically significant difference in neurogenesis between SCR vs. HAV (200 Pa) (Fig. 3A and B). Interestingly, cells in HAVDI gels exhibited lower F-actin intensity compared to SCR gels, indicating the inhibitory role of HAVDI adhesion in cytoskeletal formation. In addition, vinculin, a membrane-cytoskeletal protein in focal adhesion (FA) plaques involved in anchoring F-actin to the membrane, was immunostained to examine its distribution and expression. Vinculin for cells in the HAV gel was distributed only near or within the nucleus and dispersed less widely in protrusions compared to the SCR gel (Fig. 3C). Quantification of vinculin fluorescence intensity further showed slightly lower intensity in response to HAVDI-mediated interaction in HAV gels compared to SCR gels (Fig. 3D). We next compared signaling processes downstream of cell adhesion in HAV and SCR gels. In particular, we performed western blotting for vinculin and phosphorylated (Tyr397) focal adhesion kinase (pFAK), whose phosphorylation-mediated activation occurs upon cell adhesion.³ As HAVDI concentration increases from 0 mM to 2 mM, the expression levels of both vinculin and pFAK was slightly decreased (Fig. 3E). Furthermore, a pull-down RhoA activation assay was performed to examine if HAVDI ligation influences RhoA signaling. We utilized affinity beads linked to an effector protein that selectively binds the active GTPase forms and conducted

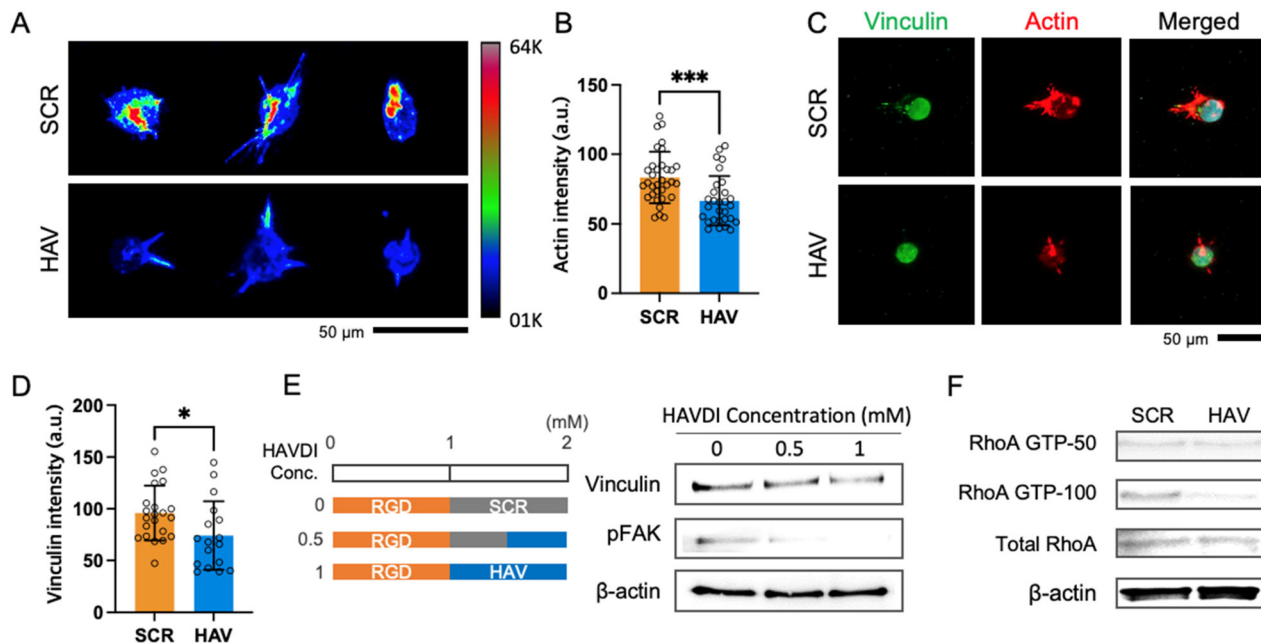


Fig. 3 N-Cadherin adhesive ligation restricts cytoskeletal formation and RhoA signaling. (A), Color-coded intensity map of phalloidin (F-actin)-stained hNSCs in SCR and HAV gels (200 Pa) at day 1. Scale bar, 50 μ m. (B), Quantification of actin intensity in hNSCs in SCR and HAV gels (200 Pa). $n > 28$ cells in each group. (C), Immunofluorescent images of single hNSC in SCR or HAV gels stained for vinculin (green), F-actin (red), and nuclei (blue). Scale bar, 50 μ m. (D), Quantification of vinculin expressions from immunofluorescent intensities in SCR and HAV gels at day 1. $n > 16$ cells in each group. (E), Composition of the gels with three different functionalized HAVDI concentration (0 mM, 0.5 mM, 1 mM) and western blotting for vinculin and pFAK in hNSCs within the three different gels. (F), RhoA activation assay of hNSCs within SCR and HAV 3D gels with 50 mM (RhoA GTP-50) and 100 mM (RhoA GTP-100) of activated RhoA GTP detecting beads. Student's *t*-test. **** $P < 0.001$, *** $P < 0.005$, ** $P < 0.01$, * $P < 0.05$. Graphs show means \pm SD.

western blotting with RhoA antibody. We utilized affinity beads with immobilized rhotekin-Rho binding domain (RBD) effector domain, for RhoA GTP pulldown, at two different concentrations (50 mM and 100 mM). The lower concentration (50 mM) of the affinity bead did not detect significant difference in the RhoA GTP level. On the other hand, with 100 mM of the beads, RhoA GTP expression level in SCR was elevated, implying that the 50 mM concentration is not high enough for sensitive detection of RhoA GTP levels in SCR and HAV gels. With 100 mM affinity beads, the expression level of RhoA GTP appeared to be slightly lower in cells within HAV gels as compared to the SCR gels, whereas total RhoA level did not show a significant difference (Fig. 3F). This indicates that RhoA signaling activation is constrained by HAVDI-mediated interaction altering cell mechanosensing state to as if it were under softer microenvironments in which the RhoA activity has been known as lower.¹⁶

Together, our results correlate well with a previous finding that N-cadherin-adhesive interaction limits actin organization and decreases FA size.³³ In that work, binding to HAVDI altered the ability of mesenchymal stem cells (MSCs) to mechanically probe their 2D substrates, reducing the contractile state of the cell. As a result, the ligation modulated the interpretation of 2D substrate stiffness cues. Furthermore,

Zhang *et al.* recently showed that this HAVDI adhesive motif interaction erases Yes-associated protein (YAP) localization-mediated mechanical memory of MSCs on 2D substrates.³² Given that NSC lineage commitment in 3D matrices is also regulated by actin cytoskeletal formation⁹ and RhoA signaling (Fig. 1E and F), the enhanced neurogenesis in HAV gels may be highly associated with the HAVDI interaction-mediated attenuation of mechanosensitive features.

2.4. HAVDI-mediated adhesion enhances β -catenin activity

We next investigated whether HAVDI-mediated adhesion influences β -catenin signaling, which is known to promote the expression of NeuroD1, a proneuronal transcription factor for NSCs.³⁷ Immunofluorescence staining of active β -catenin in hNSC encapsulated with SCR or HAV gels revealed that HAV gels exhibit not only higher expression of active β -catenin than SCR gels, but also slightly biased distribution of the expression towards cell boundary in which cadherin adhesion exists (Fig. 4A–C). Furthermore, the expression level of total β -catenin was also slightly higher in HAV gels, whereas inactive β -catenin (phosphorylated at Ser33/37/Thr41) shows the opposite trend (Fig. 4D and E). These results demonstrate that HAVDI-mediated interaction enhances β -catenin level in 3D matrices. Since β -catenin has been reported as to play a critical role in

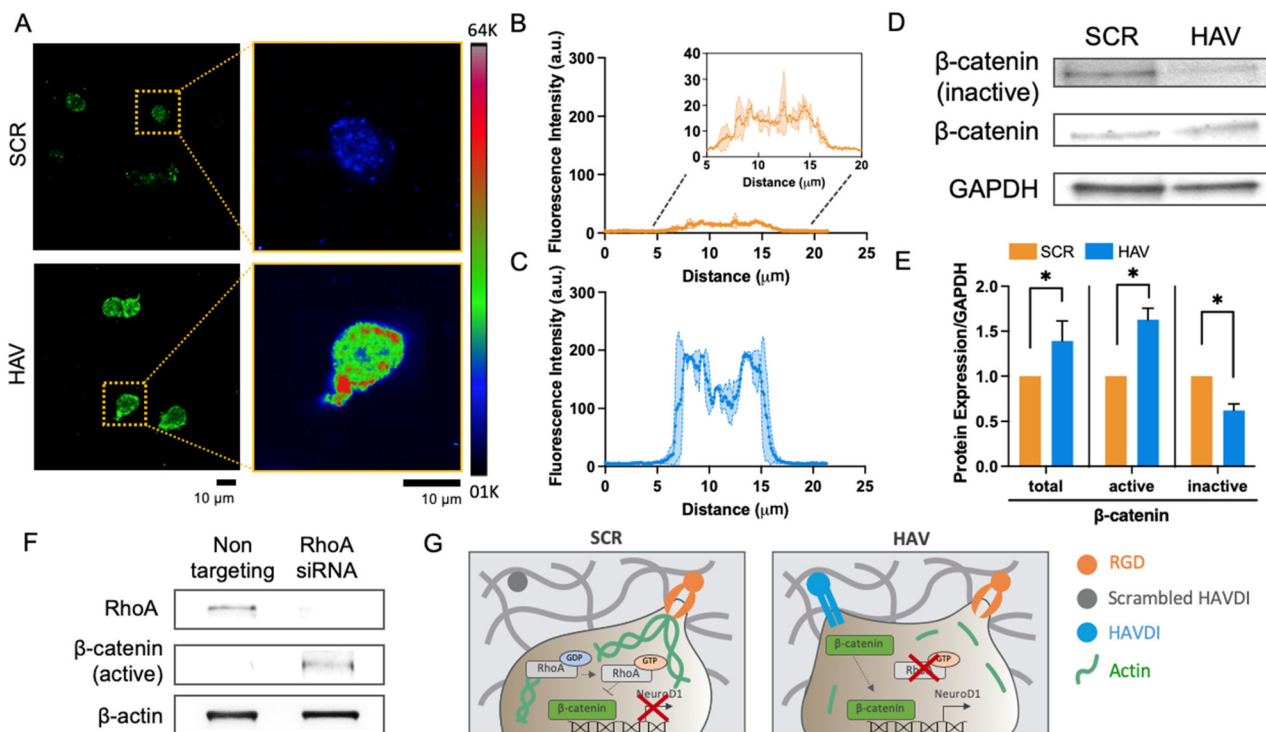


Fig. 4 N-Cadherin adhesive ligation enhances β -catenin activity in 3D matrices. (A), Immunofluorescent images and color-coded immunofluorescence intensity map of active β -catenin in hNSCs encapsulated with SCR and HAV gels. Representative subcellular distributions of active β -catenin along the lines crossing single cells encapsulated with (B), SCR and (C), HAV gels. (D), Western blotting of inactive β -catenin (phosphorylated at Ser33/37/Thr41) and total β -catenin in hNSCs after 3 days of culture in SCR and HAV gels. (E), Quantification of the western blotting for total, active, and inactive β -catenin in hNSCs encapsulated with SCR and HAV gels. $n = 2$ biological replicates. (F), Immunoblot of RhoA and active- β -catenin in non-targeting and RhoA-targeting siRNA-treated cells encapsulated in SCR gels. (G), Proposed mechanism for how HAVDI-mediated interaction enhances the neurogenesis of hNSCs within 3D matrices.

mechanosensitive NSC lineage commitment in 3D matrices as well,⁹ our finding supports the idea that HAVDI adhesion may promote neuronal differentiation by regulating β -catenin signaling.

Next, we examined whether there is any causal link between this β -catenin and RhoA signaling, which both lie downstream of HAVDI interaction. We treated hNSCs with a siRNA targeting RhoA, and the cells were encapsulated in SCR gels (200 Pa), which previously showed higher RhoA activity than those in HAV gels at the same stiffness. Interestingly, the RhoA siRNA-treated cells exhibited increased expression of active β -catenin as compared to non-targeting siRNA-treated cells (Fig. 4F). This inverse, causal link between RhoA activity and β -catenin signaling has been reported with other stem cells and cancer cell lines.^{47–49} RhoA activation by Wnt3a has been found to activate Janus kinase (Jk) and thereby directly activate glycogen synthase kinase-3 β (Gsk3 β), resulting in destabilization of β -catenin in bone marrow stem cells.⁴⁸ In human colon cancer cells, RhoA inactivation led to the redistribution of β -catenin from the membrane to the nucleus and enhanced Wnt/ β -catenin signalling.⁴⁹ Taken together, our result indicates that restricted RhoA signaling caused by HAVDI adhesion (Fig. 3F) may play a role in increasing β -catenin activity and consequently promoting neurogenesis in 3D matrices (Fig. 4G).

3. Conclusion

In this study, we developed a click chemistry-based 3D hydrogel platform with fully decoupled presentation of cell–cell and cell–ECM adhesive interactions to evaluate how these cues mutually affect to regulate NSC lineage commitment. Ligation of the HAVDI adhesive domain from N-cadherin EC1 emulated cell–cell interaction in 3D gels independently of RGD peptide ligation to simulate cell–ECM interaction. Harnessing this platform, we revealed a new biomechanical model for regulating mechanosensitive neurogenesis as a consequence of multiple adhesive interactions in 3D microenvironment. When the HAVDI interaction is co-presented with integrin-mediated RGD ligation, the HAVDI interaction biased NSC lineage commitment towards neuronal lineage in stiffer gels. Furthermore, HAVDI adhesive interaction altered the mechanical state of hNSCs by restricting cytoskeleton formation and RhoA signaling, which are generally known to be regulated by integrin-mediated cell–ECM interaction during mechanosensing. This corresponds well with previously reported attenuating role of HAVDI ligation during mechanosensing process of hMSCs on 2D substrates, demonstrating that N-cadherin adhesive interaction can ‘shield’ the cells from sensing mechanical cues. Furthermore, the HAVDI adhesive interaction facilitated β -catenin activation, which promotes neurogenesis. The β -catenin activation was increased by genetic perturbation of RhoA by siRNA, suggesting that there may be a causal link between RhoA and β -catenin signaling in 3D matrices. Collectively, our finding of mechanosensitive NSC lineage commitment and its correlation with cytoskeletal formation is

consistent with our previous study with the same 3D hydrogel materials system.⁹ Based on this, our work additionally establishes that cell–cell and cell–ECM interactions in 3D matrices can integrate to regulate mechanosensitive NSC lineage commitment especially through blocking of cell–ECM interaction-derived mechanosensing by cell–cell interaction. Moreover, our material platform could be a great general tool to observe the effect of cell–cell interaction on diverse cell behaviors within a 3D environment.

4. Experimental section

4.1 HA-DBCO synthesis

DBCO was functionalized to HA by *N*-hydroxysuccinide (NHS)-*N*-(3-dimethylaminopropyl)-*N'*-ethylcarbodiimide (EDC) chemistry.^{9,35} NHS (Sigma) and EDC (Sigma) was added to aqueous HA (average molecular weight 66–99 kDa, Lifecore Biomedical) solution and the mixed solution was incubated for 1 h. Then, dibenzocyclooctyne-amine (DBCO-amine) (Sigma) was conjugated to the solution, and reacted for 48 h. The presence of DBCO in the HA backbone was confirmed by ¹H nuclear magnetic resonance (NMR) (Advance Neo 600).

4.2 Hydrogel characterization

Swelling ratio (*Q*) of the gels were estimated by calculating the ratio of the mass of the swollen hydrogel (in DMEM overnight) to that of the dry polymer obtained by lyophilisation. Mesh size of the hydrogel polymeric network was estimated by using the Canal and Peppas method.^{40,50} The physical parameters of HA-DBCO were assumed to be the same as those of HA. Incorporation and distribution of HAVDI and scrambled HAVDI peptides were confirmed by fluorescence tagging of the peptides with NHS-fluorescein after washing with PBS for three times.

4.3 hNSC culture

hNSCs were derived from the telencephalon (HFT13) as previously described,³⁸ and the culture of the cells in undifferentiated state was performed with Dulbecco's modified Eagle's medium/Nutrient Mixture F12 (DMEM/F12) medium (Gibco) with supplements: N-2 formulation (1 v/v%, Gibco), basic fibroblast growth factor (bFGF) (20 ng mL⁻¹, Sigma), leukemia inhibitory factor (LIF) (10 ng mL⁻¹, Sigma), Heparin (8 μ g mL⁻¹, Sigma, for the stabilization of activity of the growth factors), and penicillin/streptomycin (2 v/v%, Gibco). The cells were incubated as neurospheres in humidified air with 5% CO₂ at 37 °C. Half of the growth medium was replenished every 2–3 days, and passaging was undertaken every 7–8 days by dissociation of the neurospheres.

4.4 hNSC encapsulation

DBCO-functionalized HA (HA-DBCO) formed hydrogels through stain-promoted azide alkyne cycloaddition (SPAAC), a bio-orthogonal gelation, between the azide and DBCO functional groups. Polyethylene glycol (PEG)-bis (azide) (Sigma)

was used as crosslinker for the SPAAC reaction. Encapsulation of hNSCs was performed by incubating the mixture of HA-DBCO, PEG-bis (azide), and the cells at 37 °C for 10 min. Before encapsulation, hNSCs were dissociated from neurospheres in an undifferentiated state and added to the gel mixture at a cell density of 7×10^3 cells per μL , and maintained under a culture condition without supplementation of bFGF and LIF for 4 days after encapsulation. Azido peptides including (Ac-K(N₃)-GSGRGDSPG-NH₂ (azido RGD), Ac-K(N₃)-HAVDIGGG-NH₂ (azido HAVDI), and Ac-K(N₃)-AGVGDHIGC-NH₂ (azido scrambled HAVDI)) (Peptron) were also ligated to the gel by adding them into the HA formulation before incubation, as needed. In order to regulate elastic modulus of the gels, molar ratio of azide group in PEG-bis (azide) to HA monomer was controlled. The moduli after gelation were measured by rheometer (Bohlin Advanced Rheometer Malvern Instruments, U.K.).

4.5 Immunocytochemistry

hNSCs within each gel (7×10^4 cells in a 10 μL gel) were fixed by incubating with a 4% paraformaldehyde solution (Sigma) for 15 min at room temperature (RT). Fixed cells were incubated with Triton X-100 (0.3% w/v, Sigma) and BSA (1% w/v) in D-PBS (Dulbecco's phosphate-buffered saline) solution for 30 minutes at RT, washed with D-PBS. Samples were then incubated at 4 °C for 48 h with the following primary antibodies: mouse anti-N-cadherin (1:500, C3865, Sigma), mouse anti-Tubulin β 3 (TUBB3) (1:1000, 801201, BioLegend), rabbit anti-glial fibrillary acidic protein (GFAP) (1:1000, ab7260, Abcam), and mouse anti-vinculin (1:200, ab18058, Abcam), and mouse anti-active- β -catenin (1:200, 05-665, Millipore). After washing with D-PBS, the resulting samples were stained with goat anti-mouse IgG (H+L) secondary antibody, Alexa fluor 488 (1:250, cat. no. A11001; Invitrogen) or goat anti-rabbit IgG (H+L) secondary antibody, Alexa fluor 633 (1:250, cat. no. A21070; Invitrogen) for 40 min at RT, then with 4',6-diamidino-2-phenylindole (DAPI, Sigma) for 10 minutes to counterstaining of cell nuclei. Cytoskeleton was stained with Rhodamine Phalloidin (1:40, cat. no. R415; Invitrogen). All fluorescence images were visualized by z-stack mode with a confocal laser-scanning microscope (LSM 780, Carl Zeiss).

4.6 Western blot

hNSCs encapsulated with 3D HA gel (4.9×10^5 cells in a 70 μL gel) were harvested by incubating with hyaluronidase (Sigma) at 37 °C for 10 min. RIPA lysis buffer containing a proteinase inhibitor cocktail (ThermoFisher Scientific) was treated to the cells on ice for 20 min to extract total protein. Proteins extracted from the lysate was quantified by Bradford protein assay kit (Bio-Rad) and normalized to load equal amounts of protein (15 μg) to Bolt 4–12% Bis-Tris Plus polyacrylamide gels (ThermoFisher Scientific) for separating by electrophoresis. Then, the proteins separated by electrophoresis on gels were transferred to polyvinylidene difluoride (PVDF) membranes using an iBlot2 transfer system (ThermoFisher Scientific) according to the manufacturer's instructions. The membranes

were blocked by BSA (1%) in Tris-buffered saline (TBS) (Sigma) for 40 min at RT and incubated overnight at 4 °C with following primary antibodies: mouse anti-vinculin antibody (1:500, v9131; Sigma), rabbit anti-phospho-FAK (Tyr39) antibody (1:500, 700255, ThermoFisher Scientific), mouse anti-RhoA (1:100, ab54835, Abcam), rabbit anti-phospho- β -catenin antibody (Ser33/37/Thr41) (1:1000, 9651, Cell Signaling Technology), anti-active- β -catenin antibody (1:200, 05-665, Millipore), rabbit anti- β -actin antibody (1:1000, cat. no. 4967; Cell Signaling Technology). Then the samples were treated with horseradish peroxidase (HRP)-conjugated goat anti-rabbit IgG (1:2000, act. no. ab6721; Abcam) or HRP-conjugated goat anti-mouse IgG (1:2000, cat. no. 62-6520; Invitrogen) secondary antibodies for 30 min at RT. The signals from proteins were detected using SuperSignal West Pico Chemiluminescent Substrate (ThermoFisher Scientific) and a ChemiDoc MP system (Bio-Rad).

4.7 RhoA activity assay

The RhoA activity of hNSCs within each gel was measured using respective pull-down assay kits (BK036, Cytoskeleton), and western blotting was performed to obtain a final readout.

4.8 RhoA knockdown

Knockdown for RhoA was performed by siRNA delivery. hNSCs (3×10^5 cells) in siRNA delivery media (B-005000-500, Dharmacon) was incubated with non-targeting siRNA (1 μM , D-001910-10-05, Dharmacon) or RhoA-targeting siRNA (E-003860-00-0005, Dharmacon) for 66 h. Then, the cells were harvested for western blotting.

4.9 Statistical analysis

Data are expressed as means \pm standard error of mean (s.e.m.). Statistical comparisons were conducted using an independent sample *t*-test or one-way analysis of variance (ANOVA) with Tukey *post hoc* testing used to make pairwise comparisons between multiple groups. Statistical significance was set to $p < 0.05$.

Data availability

All data supporting the findings of this study are available in the ESI files.†

Author contributions

Jieung Baek: Conceptualization, methodology, investigation, writing original draft. Sanjay Kumar: Conceptualization, funding acquisition, writing – review & editing. David V. Schaffer: Conceptualization, funding acquisition, writing – review & editing. Sung Gap Im: Writing – review & editing, funding acquisition, supervision, project administration.

Conflicts of interest

There are no conflicts to declare.

Acknowledgements

We thank K. I. Park (Yonsei University College of Medicine, Seoul) for providing us hNSCs. This work was supported by a grant from the Technology Innovation Program (No. 20008777) funded by the Ministry of Trade, Industry & Energy (MOTIE, Korea), and by the National Research Foundation of Korea (NRF) grant funded by the Korea government (MSIT) (No. 2021R1A2B5B03001416). This work was also supported by National Institutes of Health (R01NS074831 to S. K. and D. V. S.).

References

- C. Grochowski, E. Radzikowska and R. Maciejewski, *Clin. Neurol. Neurosurg.*, 2018, **173**, 8–14.
- M. J. Smith, M. Paton, M. C. Fahey, G. Jenkin, S. L. Miller, M. Finch-Edmondson and C. A. McDonald, *Stem Cells Transl. Med.*, 2021, **10**, 1621–1636.
- J. Baek, S.-Y. Cho, H. Kang, H. Ahn, W.-B. Jung, Y. Cho, E. Lee, S.-W. Cho, H.-T. Jung and S. Im, *ACS Appl. Mater. Interfaces*, 2018, **10**, 33891–33900.
- J. Baek, W.-B. Jung, Y. Cho, E. Lee, G.-T. Yun, S.-Y. Cho, H.-T. Jung and S. Im, *ACS Appl. Mater. Interfaces*, 2019, **11**, 17247–17255.
- L. Gómez-Virgilio, G. Ramírez-Rodríguez, C. Sánchez-Torres, L. Ortiz-López and M. Meraz-Ríos, *Mol. Neurobiol.*, 2018, **55**, 8014–8037.
- H. Yang, J. Wang, F. Wang, X. Liu, H. Chen, W. Duan and T. Qu, *Dopaminergic Neuronal Differentiation from the Forebrain-Derived Human Neural Stem Cells Induced in Cultures by Using a Combination of BMP-7 and Pramipexole with Growth Factors*, 2016, vol. 10, p. 29.
- Z. Z. Khaing and S. K. Seidlits, *J. Mater. Chem. B*, 2015, **3**, 7850–7866.
- L. Pous, S. S. Deshpande, S. Nath, S. Mezey, S. C. Malik, S. Schildge, C. Bohrer, K. Topp, D. Pfeifer, F. Fernández-Klett, S. Doostkam, D. K. Galanakis, V. Taylor, K. Akassoglou and C. Schachtrup, *Nat. Commun.*, 2020, **11**, 630.
- J. Baek, P. A. Lopez, S. Lee, T.-S. Kim, S. Kumar and D. V. Schaffer, *Sci. Adv.*, 2022, **8**, eabm4646.
- K. Yang, J. Lee, J. Kim, Y. Lee, H. Shin, S. Um, J. Kim, K. Park, H. Lee and S.-W. Cho, *Biomaterials*, 2012, **33**, 6952–6964.
- R. S. Ashton, A. Conway, C. Pangarkar, J. Bergen, K.-I. Lim, P. Shah, M. Bissell and D. V. Schaffer, *Nat. Neurosci.*, 2012, **15**, 1399–1406.
- Q. Jiao, X. Li, J. An, Z. Zhang, X. Chen, J. Tan, P. Zhang, H. Lu and Y. Liu, *Front. Cell. Neurosci.*, 2017, **11**, 200.
- J. F. Cherry, N. K. Bennett, M. Schachner and P. V. Moghe, *Acta Biomater.*, 2014, **10**, 4113–4126.
- A. Haque, N. Adnan, A. Motazedian, F. Akter, S. Hossain, K. Kutsuzawa, K. Nag, E. Kobatake and T. Akaike, *PLoS One*, 2015, **10**, e0135170.
- S. Rammensee, M. S. Kang, K. Georgiou, S. Kumar and D. V. Schaffer, *Stem Cells*, 2016, **35**, 497–506.
- A. J. Keung, E. M. de Juan-Pardo, D. V. Schaffer and S. Kumar, *Stem Cells*, 2011, **29**, 1886–1897.
- P. H. Kang, D. V. Schaffer and S. Kumar, *Mol. Biol. Cell*, 2020, **31**, 386–396.
- A. Banerjee, M. Arha, S. Choudhary, R. S. Ashton, S. R. Bhatia, D. V. Schaffer and R. S. Kane, *Biomaterials*, 2009, **30**, 4695–4699.
- Y. Zhu, X. Li, R. R. Janairo, G. Kwong, A. D. Tsou, J. S. Chu, A. Wang, J. Yu, D. Wang and S. Li, *J. Cell. Physiol.*, 2019, **234**, 7569–7578.
- Y. Ryu, M. Iwashita, W. Lee, K. Uchimura and Y. Kosodo, *Front. Aging Neurosci.*, 2021, **13**, 709620.
- C. Kothapalli, G. Mahajan and K. Farrell, *Biomater. Sci.*, 2020, **8**, 5452–5464.
- S. Wu, R. Xue, B. Duan and P. Jiang, *J. Mater. Chem. B*, 2017, **5**, 3870–3878.
- R. Y. L. Tsai and R. D. G. McKay, *J. Neurosci.*, 2000, **20**, 3725–3735.
- J. Tang, R. Peng and J. Ding, *Biomaterials*, 2010, **31**, 2470–2476.
- B. M. Baker and C. S. Chen, *J. Cell Sci.*, 2012, **125**, 3015–3024.
- S. R. Caliarì, S. L. Vega, M. Kwon, E. M. Soulas and J. A. Burdick, *Biomaterials*, 2016, **103**, 314–323.
- M. Bao, J. Xie and W. T. S. Huck, *Adv. Sci.*, 2018, **5**, 1800448.
- E. Cukierman, R. Pankov, D. R. Stevens and K. M. Yamada, *Science*, 2001, **294**, 1708–1712.
- J. Y. Lee, J. K. Chang, A. A. Dominguez, H.-p. Lee, S. Nam, J. Chang, S. Varma, L. S. Qi, R. B. West and O. Chaudhuri, *Nat. Commun.*, 2019, **10**, 1848.
- S. D. Skaper, L. Facci, G. Williams, E.-J. Williams, F. S. Walsh and P. Doherty, *Mol. Cell. Neurosci.*, 2004, **26**, 17–23.
- G. Williams, E.-J. Williams and P. Doherty, *J. Biol. Chem.*, 2002, **277**, 4361–4367.
- C. Zhang, H. Zhu, X. Ren, B. Gao, B. Cheng, S. Liu, B. Sha, Z. Li, Z. Zhang, Y. Lv, H. Wang, H. Guo, T. Lu, F. Xu, G. M. Genin and M. Lin, *Nat. Commun.*, 2021, **12**, 6229.
- B. D. Cosgrove, K. L. Mui, T. P. Driscoll, S. R. Caliarì, K. D. Mehta, R. K. Assoian, J. A. Burdick and R. L. Mauck, *Nat. Mater.*, 2016, **15**, 1297–1306.
- W. Su, S. Matsumoto, B. Sorg and L. S. Sherman, *Matrix Biol.*, 2019, **78–79**, 272–283.
- M. M. Adil, T. Vazin, B. Ananthanarayanan, G. Rodrigues, A. T. Rao, R. U. Kulkarni, E. W. Miller, S. Kumar and D. V. Schaffer, *Biomaterials*, 2017, **136**, 1–11.
- G. Dréau and E. Martí, *Dev. Neurobiol.*, 2012, **72**, 1471–1481.

- 37 L. Zhang, X. Yang, S. Yang and J. Zhang, *Eur. J. Neurosci.*, 2011, **33**, 1–8.
- 38 H.-T. Kim, I.-S. Kim, I.-S. Lee, J.-P. Lee, E. Y. Snyder and K. Park, *Exp. Neurol.*, 2006, **199**, 222–235.
- 39 C. M. Madl and S. C. Heilshorn, *Adv. Funct. Mater.*, 2018, **28**, 1706046.
- 40 B. Ananthanarayanan, Y. Kim and S. Kumar, *Biomaterials*, 2011, **32**, 7913–7923.
- 41 M. N. Collins and C. Birkinshaw, *J. Appl. Polym. Sci.*, 2008, **109**, 923–931.
- 42 B. Mersman, W. Zaidi, N. I. Syed and F. Xu, *Front. Synaptic Neurosci.*, 2020, **12**, 29.
- 43 M. Machacek, L. Hodgson, C. Welch, H. Elliott, O. Pertz, P. Nalbant, A. Abell, G. L. Johnson, K. M. Hahn and G. Danuser, *Nature*, 2009, **461**, 99–103.
- 44 A. Hall, *Science*, 1998, **279**, 509–514.
- 45 B.-A. Truong Quang, M. Mani, O. Markova, T. Lecuit and P.-F. Lenne, *Curr. Biol.*, 2013, **23**, 2197–2207.
- 46 D. Fichtner, B. Lorenz, S. Engin, C. Deichmann, M. Oelkers, A. Janshoff, A. Menke, D. Wedlich and C. M. Franz, *PLoS One*, 2014, **9**, e93123.
- 47 G. Yan, R. Zou, Z. Chen, B. Fan, Z. Wang, Y. Wang, X. Yin, D. Zhang, L. Tong, F. Yang, W. Jiang, W. Fu, J. Zheng, M. O. Bergo, M. Dalin, J. Zheng, S. Chen and J. Zhou, *Acta Biochim. Biophys. Sin.*, 2014, **46**, 682–690.
- 48 W. Shi, C. Xu, Y. Gong, J. Wang, Q. Ren, Z. Yan, L. Mei, C. Tang, X. Ji, X. Hu, M. Qv, M. Hussain, L.-H. Zeng and X. Wu, *Cell Regener.*, 2021, **10**, 8.
- 49 P. Rodrigues, I. Macaya, S. Bazzocco, R. Mazzolini, E. Andretta, H. Dopeso, S. Mateo-Lozano, J. Bilić, F. Cartón-García, R. Nieto, L. Suárez-López, E. Afonso, S. Landolfi, J. Hernandez-Losa, K. Kobayashi, S. y. Cajal, J. Taberner, N. C. Tebbutt, J. M. Mariadason, S. Schwartz and D. Arango, *Nat. Commun.*, 2014, **5**, 5458.
- 50 T. Canal and N. A. Peppas, *J. Biomed. Mater. Res.*, 1989, **23**, 1183–1193.